Charge heteroaggregation between hard and soft particles

A. Fernández-Barbero[1,*] and B. Vincent[2,†]
[1]*Complex Fluid Physics Group, Department of Applied Physics, University of Almería, Cañada de San Urbano s/n, E-04120 Almería, Spain*
[2]*School of Chemistry, University of Bristol, Cantock's Close, Bristol BS8 1TS, United Kingdom*
(Received 1 June 2000; published 22 December 2000)

In this paper, the heteroaggregation of opposite sign hard and soft colloidal particles has been studied by static and dynamic light scattering. The structure of the aggregates, as well as the aggregation kinetics, have been investigated. At low electrolyte concentration, where both long-range electrostatic repulsive and attractive forces are present, the aggregates were found to be more open than expected for diffusion-limited cluster aggregation (DLCA). However, the aggregate size time evolution is characteristic of diffusion-controlled processes. At high electrolyte concentration, where DLCA would be expected, very compacted clusters were found, as well as very rapid aggregation, leading to high polydispersity. These latter findings are interpreted in terms of the differences in the homoaggregation speeds for the hard and soft particles.

DOI: 10.1103/PhysRevE.63.011509 PACS number(s): 82.70.Dd, 64.60.Cn, 05.40.−a

INTRODUCTION

The structure of colloidal aggregates has attracted much research interest since it was shown that the concept of fractals can be used to characterize the structure of random clusters growing under nonequilibrium conditions [1]. For many colloidal dispersions, certain limiting values of the fractal dimension have been found. For example for dispersions of gold, silica and polystyrene particles, $d_f \approx 1.75$ under diffusion-controlled conditions, and $d_f \approx 2.0$ when the aggregation occurs in the presence of an energy barrier [2]. Moreover, a linear increase of the mean cluster size in time is characteristic for processes dominated by cluster diffusion, whilst, in the presence of an energy barrier, the mean cluster size increases with time as a power law with an exponent larger than one. These two universal behaviors are known as diffusion-limited cluster aggregation (DLCA) and reaction-limited cluster aggregation (RLCA), respectively [3,4]. In intermediate regions, a continuous variation between these two limiting cases is usually found.

Heteroaggregation is a special type of particle aggregation in which certain asymmetries are involved. For example, variations in the aggregation rate constant for dimer formation occur when particles with different sizes coagulate [5]. However, this initial asymmetry does not seem to affect the cluster-size distribution after long aggregation times [6].

In the present paper, the aggregation of an equal number of positive and negative particles is reported. At low electrolyte concentration, the long-range electrostatic forces are attractive between particles of opposite sign and repulsive between those of the same sign. Due to the presence of repulsive as well as attractive forces within the aggregates, more open clusters might be expected, compared to homocoagulation under DLCA conditions. The main difference in the current work, with respect to previous papers [7–9], is the presence of an extra asymmetry, appearing when the negative particles are hard spheres, and the positive ones are soft particles. This fact modifies the short-range forces, responsible for stable bond formation, altering the aggregation kinetics and cluster morphology.

Static and dynamic light scattering were employed to determine the structure of the aggregates and to study the kinetics of the aggregation processes, respectively. Furthermore, phase contrast optical microscopy was used for direct observations. The ionic concentration was used to control both the strength and the range of the interactions. Thus, at low electrolyte concentrations, long-range electrostatic forces dominate the kinetics as well as the aggregate structure, whilst at high electrolyte concentrations, the shorter-range van der Waals interactions may be expected to control the aggregation behavior.

The outline of this paper is as follows: The first section is a brief summary about the experimental methods employed to determine the cluster structure and the growth kinetics, together with instrumental details. The second section describes the experimental systems used and their basic characterization. The third section contains the experimental results and a discussion of these.

I. EXPERIMENTAL METHODS: BACKGROUND THEORY

A. Static light scattering

Static light scattering (SLS) allows the cluster fractal dimension, $\mathbf{d}_f$, to be determined from the angular dependence of the mean scattered intensity. For elastic scattering, the scattered light intensity from a system of clusters may be expressed in a factorized form as [10]:

$$I(q) \sim P(q)S(q), \tag{1}$$

where $q = 4\pi/\lambda \sin(\theta/2)$ is the scattering wave vector, with λ being the wavelength of the light in the solvent and θ the scattering angle. The form factor, $P(q)$, is related to the particle size and shape. The structure factor, $S(q)$, depends on the relative positions of the particles within the clusters and hence, contains the information about the structure. In

*Email address: AFERNAND@UAL.ES
†Email address: BRIAN.VINCENT@BRISTOL.AC.UK

the $qR \gg 1$ limit, where R is the mean aggregate size, a power law in the scattering vector is found from which, the fractal dimension may be determined. The structure factor is defined only for distances larger than the particle size and thus, that power law is only valid under the condition $qR_0 < 1$, with R_0 being the monomer size. In this scattering region, the influence of the particle form factor can be neglected and the angular variation of the intensity is related only to the cluster structure [11]:

$$I(q) \sim q^{-d_f}, \qquad qR_0 < 1 \ll qR. \tag{2}$$

For higher q values, the length scale corresponds to individual spheres within the clusters and the intensity is related to the particle form factor. In lower-q regions, topological length correlations between clusters could be studied.

B. Dynamic light scattering

Information about the aggregation kinetics can be extracted from the time evolution of the mean hydrodynamic radius, which evolves as a power law in the time for a sufficiently long time [12]:

$$\langle R_h \rangle \sim t^{\beta}, \qquad \beta = \frac{z}{d_f}. \tag{3}$$

The kinetic exponent z, contains information on the aggregation mechanism. z is one for DLCA, describing a size-independent cluster activity. When $z > 1$, the clustering between larger aggregates dominates and the mean cluster mass increases faster than under diffusion conditions. On the other hand, for $z < 1$, the activity of the smaller clusters is greater and the mean cluster mass increases more slowly than for pure diffusion-controlled processes. When energy barriers are present, the larger aggregates are more active than the smaller ones. Thus, $z > 1$ for RLCA, existing a wide range of values for z in the literature, being this fact associated with the difficulty of establishing the repulsion-controlled aggregation limit [12–16].

It is interesting to point out that the exponent z depends only on the kinetics of aggregation, whilst β contains also information about the cluster structure. For example in the case of homogeneous kernels (most frequently used coagulation kernels reported in the literature), and for nongelling systems, the exponent z is related to the homogeneity exponent λ by, $z = 1/1\text{-}\lambda$ [3,17]. This parameter describes the tendency of a large cluster to join up with another large cluster. Kernels with $\lambda \leqslant 1$ correspond to nongelling systems, i.e., an infinite cluster is formed at infinite time. λ takes the value 0 for DLCA, and 1 in the case of RLCA.

C. Experimental methods

The dynamic light scattering (DLS) experiments were performed using a slightly modified Malvern 4700 System (UK) working with a 632 nm wavelength HeNe laser. The intensity autocorrelation functions were determined at different times during aggregations. The scattering angle was set at 60° for both homo and heteroaggregation experiments. The mean hydrodynamic radius was obtained as a function of time, as well as the system polydispersity, using cummulant analysis.

For static light scattering (SLS), the mean scattered intensity was obtained for different angles in the range 20°–140°. When the final cluster structure was totally established, the mean intensity, $I(q)$, showed an asymptotic time-independent behavior, as predicted theoretically. From these asymptotic curves, the fractal dimensions were determined.

Optical microscopy experiments were carried out using an optical transmission phase contrast Nikon microscope (Japan). Pictures were captured directly by a CCD camera (Intellicam, U.S.A.) and no image treatment was applied.

TABLE I. Summary of particle characteristics. Sizes and mobilities were determined at pH=6, for which the microgel particles are in the collapsed state, and 1 mM NaCl. CCC, values were determined for NaCl.

Sample	Diameter (nm)	Mobility ($\times 10^8$ m^2 V^{-1} s^{-1})	C C C (mM)
PL^-	225± 10	−1.2± 0.1	≈400
MG^+	205± 14	1.0± 0.1	≈20

II. EXPERIMENTAL SYSTEMS

Two systems of spherical particles, with similar sizes and surface charges, were used for the heteroaggregation experiments. PL^- is an aqueous suspension of charged surfactant-free polystyrene microspheres, synthesized by emulsion polymerization of styrene, using sodium persulfate as initiator [18]. The negative particle charge arises from sulfate groups on the surface.

MG^+ is an aqueous cationic microgel suspension synthesized by the polymerization of poly(2-vinylpyridine), crosslinked with divinylbenzene (0.25 weight %). The initiator used was 2,2′-azobis(2-amidinopropane) dihydrochlride (V50, Wako) [19]. Two types of groups are able to confer charge to the colloidal particles: amidininum groups arising from the initiator, located essentially at the periphery of the particles, and the constituent monomer 2VP, uniformly distributed within the particles. The pK_a of 2VP is 5, and that of the amidinium groups around ten [20]. Therefore, for pH higher than five, the particles are in their collapsed state, where the bulk of the particles is totally discharged and only surface charge is present.

Samples were cleaned by serum replacement (PL^-) and dialysis (MG^+). Table I summarizes some characteristics of the experimental systems. Particle sizes were measured by transmission electron microscopy, which showed the particles to be spherical and highly monodisperse. The stability was estimated by determining the critical coagulation concentration (CCC) from the mean particle size as a function of the salt concentration (see Fig. 2 for details). Systems present different stabilities, which allows the interactions and thus

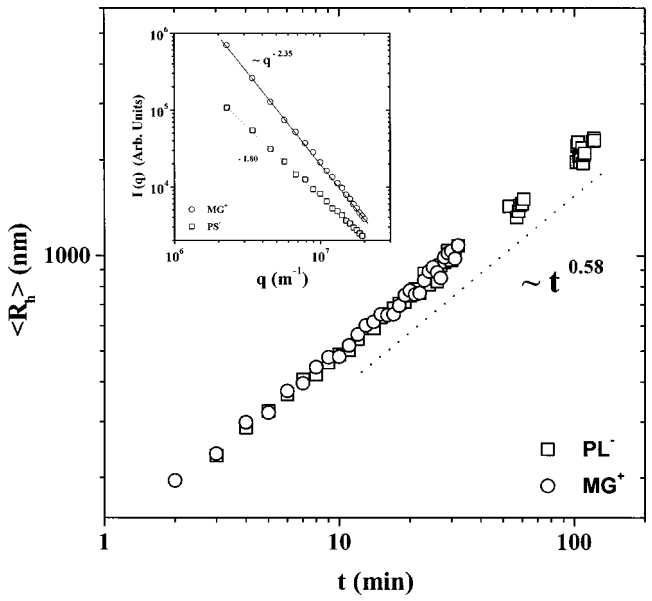

FIG. 1. Power law dependence of the mean cluster-radius with time. The mean scattered intensity for homoaggregation of both systems are also plotted at the upper-left-hand corner. The intensity curves correspond to aggregation times of 30 min and 42 min for MG^+ and PL^-, respectively.

the aggregation between different particles to be controlled through the electrolyte concentration.

The sign of the particles was studied through electrophoresis measurements, determined by phase analyzing light scattering (PALS) [21]. The mobility was negative for the system PL^- and positive for the particles MG^+, confirming the sign of the surface charge. Furthermore, the obtained values are not very different, ensuring that no important charge asymmetry is present. The mobility was observed to be pH independent for both systems in a wide range around $pH=6$, at which the aggregation experiments were performed. For more details about the particle characterization see [22].

In the aggregation experiments, sonication was always applied prior to the experiments to help ensure no aggregated particles were present initially. The particle concentration was $1.0\times10^9\,cm^{-3}$ in every case. The salt employed was NaCl (Merck, analytical grade), and temperature was always set to $(20\pm1)\,°C$.

III. RESULTS AND DISCUSSION

A. Homoaggregation

Before the heteroaggregation experiments, both systems were examined under well-known conditions, i.e., DLCA. For the experiments, both PL^- and MG^+ were coagulated independently adding NaCl at a concentration of 750 mM (above the CCC). Figure 1 shows that both systems exhibit similar behaviors for the average particle size, following a power law in the time with exponent $\beta=0.58\pm0.02$, in agreement with the long-time scaling solution [Eq. (3)]. Using static light scattering, decreasing long-time asymptotic power laws for the mean scattered intensities were obtained in both cases, indicating a regular fractal structure, being the fractal dimensions quite different: $\approx1.80\pm0.02$ for PL^- and $\approx2.35\pm0.06$ for MG^+. The former is commonly accepted for DLCA. However, the second value indicates that very compact clusters grow for the microgel particles. This finding could be related with the fact that the short-range van der Waals attraction force, responsible for the stability of the cluster structure, is weaker for the microgel particles since, even those the particles are in their collapsed state (in water), an inner structure keeps into the monomers, as demonstrated by Crowther *et al.* [23] by measuring the monomer size for different solvents (mixtures alcohol-water).

Using the values of β and the cluster fractal dimensions, the exponent z was calculated using Eq. (3) to be (1.06 ± 0.03) for the polystyrene hard spheres, as expected for diffusion-controlled aggregation. However, for the microgel particles, the kinetic is faster, leading to a kinetic exponent, $z=(1.41\pm0.04)$. This indicates that, in presence of a high salt concentration, there are two homoaggregation velocities, one for the microgel and one for the polystyrene particles. This feature will be employed in this work to design the experiments in which, one of the species coagulates faster than the other one, originating interesting results, far from classic behaviors.

The rapid kinetic observed for the microgel particles could be related to the different solvency of the polymer, with respect to that of polystyrene, that could originate extra aggregating forces. At this moment, no model is available for explaining the interactions responsible for this unexpected result. Nevertheless, this behavior agrees completely with the heteroaggregation experiments presented later, predicting the experimental heteroaggregation behavior.

B. Heteroaggregation

In the present paper, the aggregation of positive and negative particles is emphasized. Thus, particle aggregation is performed under the influence of two long-range forces: an attractive electrical force between particles of a different sign and a repulsive one, between those with the same sign.

Heteroaggregation of an equal initial number of particles of each species was tackled to simplify methods. Under this condition, no extra asymmetry needs to be taken into account. The balance between the attraction and repulsive forces was performed through the amount of salt added. This is possible because of the different stability of the systems. Figure 2 shows the average particle radius determined after 24 hours by DLS, as a function of the electrolyte concentration for both systems. For concentrations above the CCC (labeled in the plot), the particles were observed to be totally coagulated. Three aggregation regions can be defined. In Region 1, both systems are stable (salt concentration below both CCC values). The aggregation between particles of opposite sign should occur under the influence of electrostatic attraction forces. In Region 2, the positive particles start homoaggregation while the negative ones do not homocoagulate. The positive-positive encounters should be diffusive, as well as the positive-negative ones. Moreover, negative-negative encounters are excluded by the electrostatic repul-

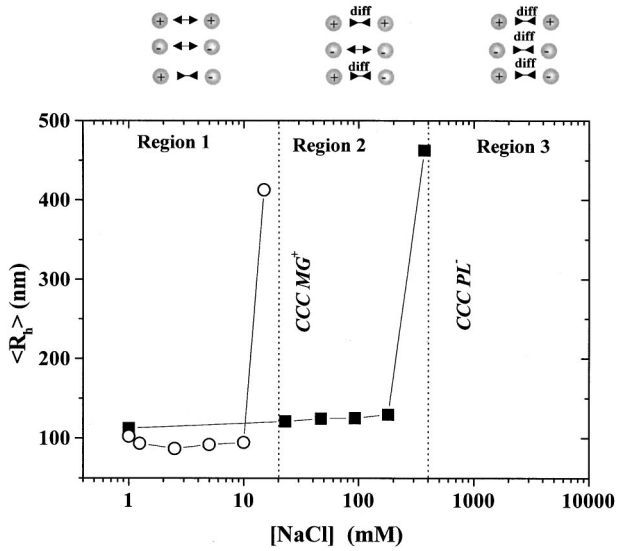

FIG. 2. Stability of the dispersions, ○ MG+ and ■ PL^-. Delineating of the aggregation regions. The upper scheme indicates the permitted and forbidden reactions in the different regions. 'diff' stands for diffusion-controlled reactions.

sion. In Region 3, the salt concentration is larger than the CCC values for both types of particles.

Figure 3 shows the time evolution of the mean radius for three selected runs. All the curves exhibit a power law in time. This means that the dynamic scaling solution for the Smoluchowski equation is also suitable for describing heteroaggregation processes in diluted systems. In Fig. 4 the mean cluster size has been plotted as a function of the salt concentration for a selection of aggregation times.

In Region 1 (Fig. 4), the size evolution of the aggregates is independent of the bulk ionic concentration, as expected. In this case, the only positive-negative encounters are possible, which are faster than diffusion. In addition, the repulsion between particles with similar signs forbids homoaggregation. Hence, a competition between these two effects must control the aggregation. It is interesting to point out that for heteroaggregation at low salt concentration (1 mM), the clusters are observed to be larger than those growing under DLCA (Fig. 3). This size difference can be due to changes of the aggregation kinetics and/or a modification in the particle structure (compactness). In order to answer this question, the fractal dimensions were also determined for heteroaggregation and the results will be presented later.

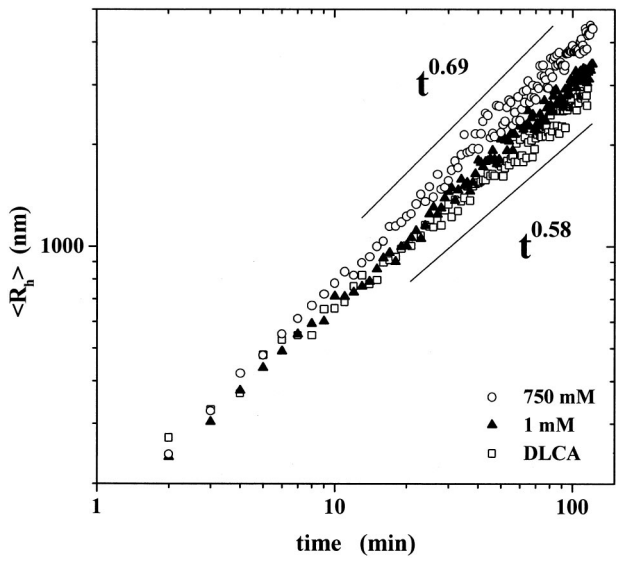

FIG. 3. Evolution of the mean radius for two selected heteroaggregation experiments. DLCA is plotted for comparison.

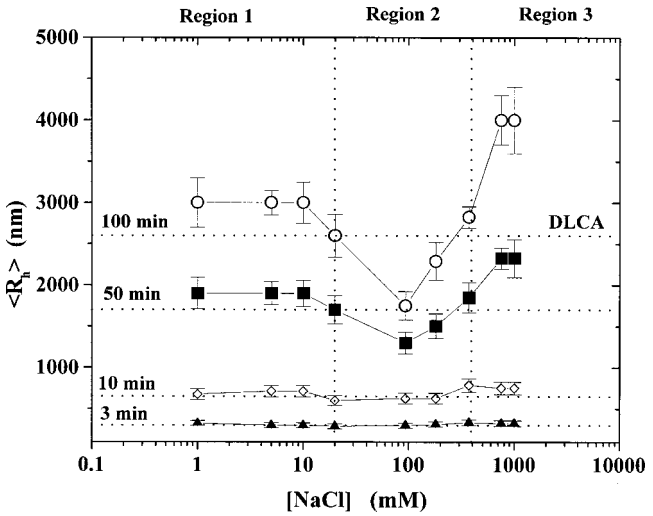

FIG. 4. Mean cluster radii for heteroaggregation, as a function of the ionic concentration, at different times. Horizontal dashed lines represent the size for clusters growing under DLCA, for the indicated times.

In Region 2, the mean cluster size is sensitive to the salt concentration (Fig. 4). Now, the positive particles are able to homocoagulate by diffusion, since the charge repulsion has been screened. For, the same reason, the negative-positive aggregation should also be diffusive. However, repulsion between any two negative particles occurs, since the charge repulsion is not screened yet. Hence, a diffusive process, in which not all the particles are reactive, occurs. The characteristic aggregation time diminishes, and the evolution of the mean cluster size is slower than for pure diffusion. This effect is observed by a decrease of the mean cluster size.

Finally, when the charge for both types of particles is totally screened (Region 3), the aggregation is again salt independent. However, an interesting result becomes apparent: the cluster size for the aggregates in Region 3 is much larger than for DLCA (see also Fig. 3).

For informative data interpretation, a second independent technique must be employed either to determine the cluster structure, or to characterize the aggregation kinetics (remember that the exponent β, obtained from the time evolution of the mean cluster size [Eq. (3)] contains information, not only on the kinetics of aggregation, but also on the cluster structure). In this work, the fractal dimension has been determined using static light scattering. Figure 5 shows the angular dependence of the mean scattered intensity, for different heteroaggregation processes. The fractal dimensions from the slopes are plotted as a function of the salt concentration, at the upper-right-hand corner. Moreover, the d_f values for

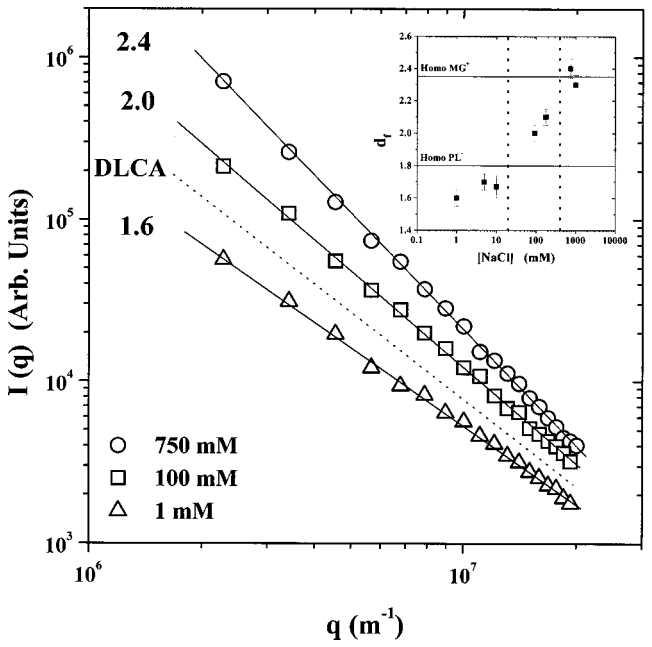

FIG. 5. SLS measurements for heteroaggregation. The slopes depend on the salt concentration, indicating different fractal structures. DLCA is also plotted for comparison. The fractal dimension as a function of the salt concentration for the heteroaggregation processes is also plotted at the upper-right-hand corner. The fractal dimensions for the homoaggregation of MG^+ and PL^- at 750 mM are also plotted for comparison.

the homoaggregation of PL^- and MG^+ under DLCA conditions are also plotted as reference.

In Region 1 a fractal dimension 1.60 ± 0.05 was found for the lowest salt concentration (1 mM), indicating a significant reduction compared to the fractal dimension for DLCA processes (1.80 ± 0.02). This result indicates that clusters growing under the influence of long-range attraction and repulsion forces are more branched than those obtained from a simple diffusion process. This result is expected: although large clusters have to be globally neutral in charge, the charge distribution is inhomogeneous. The repulsion between particles with a similar sign within the clusters favors their separation, making the clusters more branched. This decrease in the fractal dimension is consistent with the increase of size observed in Fig. 3.

At higher salt concentrations, the fractal dimension raises monotonously up to (2.40 ± 0.06) for 750 mM. Thus, the clusters show very compact structures. It is interesting to remember that the homoaggregation of system PL^- leads to $d_f \sim 1.80$, while the homoaggregation of system MG^+ leads to $d_f \sim 2.35$, and no direct information is known only for pure heteroaggregation of PS^- with MG^+. Thus, the value for heteroaggregation at high salt concentration indicates that the compact clusters coming from the homoaggregation between microgel particles have a very relevant weigh in the average, and the observed fractal dimension is mainly due to the presence of those clusters. Although the aggregate structure is more compact, an increase in the cluster size was observed (see Fig. 3). This implies that a change to faster kinetics must be occurring.

TABLE II. Kinetic exponent for heteroaggregation process as a function of salt concentration.

[NaCl] (mM)	Exponent z
1	1.04 ± 0.03
5	1.10 ± 0.02
10	0.92 ± 0.03
93	1.11 ± 0.05
180	1.17 ± 0.03
750	1.66 ± 0.01
1000	1.61 ± 0.03

Table II lists the exponent z values obtained from the exponent β and d_f. At low salt concentration, where the long-range attraction forces are particularly relevant, the exponent z is similar to that for DLCA. The aggregation due to the attraction between particles with different signs is being compensated by the absence of aggregation originated by repulsion between those with similar signs, being the overall aggregation speed not far from the diffusive one. Therefore, the difference in the cluster size evolution for heteroaggregation at low salt concentration (Fig. 3), is a consequence only of the different cluster compactness since no real difference in the aggregation kinetics is observed.

The value for high salt concentration (750 mM) indicates important changes in the kinetic process. This fact is, once again, a consequence of the difference between the homocoagulation of microgel and polystyrene particles. Thus, the aggregation reactions, in which the microgel particles are involved, dominate the overall rate of aggregation. Moreover, the exponent for the microgel homoaggregation was observed to be $z = (1.41 \pm 0.04)$, while for heteroaggregation, $z = (1.61 \pm 0.03)$, indirectly indicating that the aggregation between the negative polystyrene spheres and the posi-

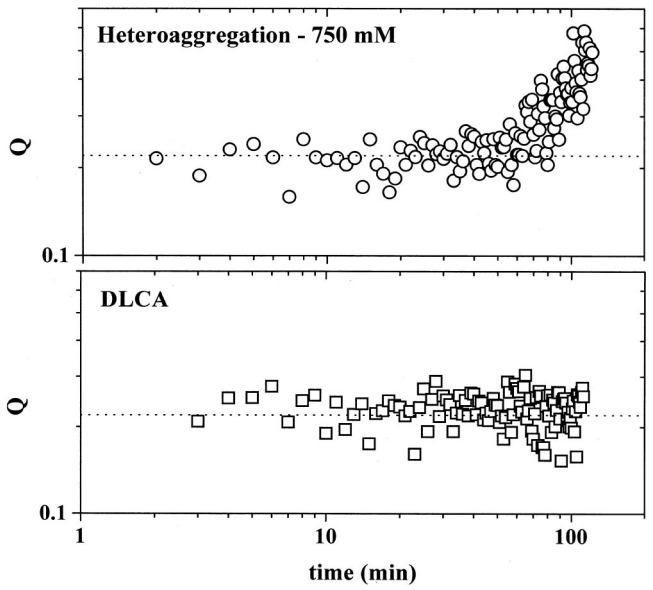

FIG. 6. Time evolution of the polidispersity for heteroaggregation at high salt concentration and DLCA.

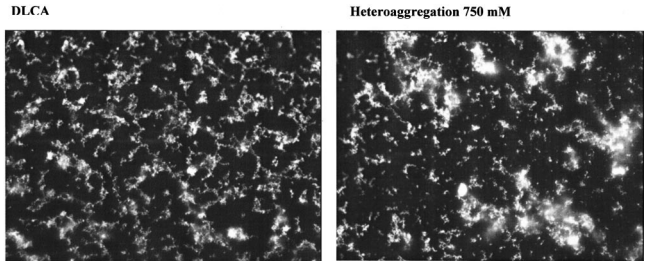

FIG. 7. Pictures of aggregated samples by transmission phase contrast optical microscopy.

tive microgel spheres is faster than for DLCA.

In order to support this finding, the polydispersity, $Q = \mu_1/2\mu_2^2$, obtained from the first and second cummulants (μ_1 and μ_2, respectively), was monitored. The results are plotted in Fig. 6, where a dramatic increase in the polydispersity is observed at long times. The polydispersity for DLCA is also plotted for comparison. The difference between the homocoagulation velocities allows large and small clusters to be simultaneously present in the scramble, leading to a high polydispersity when a sufficient number of large clusters have formed.

In order to gain further evidence of this long-time behavior at high salt concentration, transmission phase contrast optical microscopy was used to make direct observations of the aggregates. Figures 7 show pictures corresponding to DLCA, and heteroclusters, growing at high salt concentration. A more polydisperse system is clearly observed in the second case. Finally, the explanation based on differences in the homoaggregation velocities implies that the larger clusters should be formed mainly by microgel particles (or microgel-polystyrene particles), while the smaller clusters should be composed mainly by polystyrene monomers. Computer simulations and labeling experimental techniques are being currently carried out to investigate this prediction.

CONCLUSIONS

Charge colloidal heteroaggregation between an equal amount of hard and soft particles has been studied by static and dynamic light scattering. The different reactions present in heteroaggregation were controlled by the amount of salt added, since the stabilities of the systems are quite different. In addition, the strength and range of the interactions was also controlled. Thus, at low salt concentration, where the long-range electrostatic interactions dominate, the aggregates show open fractal structures and a kinetic behavior typical for DLCA, as a consequence of the compensation between the increasing velocity due to pure heteroaggregation and stopped homoaggregation reactions. However, at high salt concentration, where the short-range interactions are relevant, the heteroclusters become very compacted, with the aggregation kinetics being extremely fast. These findings are explained accounting for differences between the homoaggregation speeds for both systems. This asymmetry allows large clusters formed from the homoaggregation of the microgel particles to be present at the same time that small aggregates form to the aggregation of the polystyrene particles (sufficiently long time). This fact provokes an increase of the polydispersity, observed by dynamic light scattering an optical microscopy.

ACKNOWLEDGMENTS

The authors would like to thank Dr. A. Loxley for the synthesis of the cationic particles. A.F.B. acknowledges financial support through the University of Almería (Plan Propio de Investigación) and Andalusian Government, for supporting a one-year stay at the University of Bristol. This work was supported by CICYT (Spain), Project No. MAT2000-1550-C03-02).

[1] T. A. Witten and L. M. Sander, Phys. Rev. Lett. **47**, 1400 (1981).
[2] See for example, M. Carpineti and M. Giglio, Adv. Colloid Interface Sci. **46**, 13 (1990).
[3] M. L. Broide and R. J. Cohen, Phys. Rev. Lett. **64**, 2026 (1990).
[4] A. Fernández-Barbero, M. Cabrerizo-Vílchez, R. Martínez-García, and R. Hidalgo-Álvarez, Phys. Rev. E **53**, 4981 (1996).
[5] W. Hatton, P. McFadyen, and A. L. Smith, J. Chem. Soc., Faraday Trans. 1 **70**, 665 (1974).
[6] A. Fernández-Barbero, A. Schmitt, M. Cabrerizo-Vílchez, R. Martínez-García, and R. Hidalgo-Álvarez, Phys. Rev. E **56**, 4337 (1997).
[7] A. M. Puertas, J. A. Maroto, A. Fernández-Barbero, and F. J. de las Nieves, Phys. Rev. E **59**, 1943 (1999).
[8] A. M. Puertas, A. Fernández-Barbero, and F. J. de las Nieves, Comput. Phys. Commun. **121**, 353 (1999).
[9] A. M. Puertas, A. Fernández-Barbero, and F. J. de las Nieves (unpublished).
[10] J. K. G. Dhont, *An Introduction to Dynamics of Colloids* (Elsevier, Amsterdam, 1996).
[11] M. Y. Lin, H. M. Lindsay, D. A. Weitz, R. C. Ball, R. Klein, and P. Meakin, Phys. Rev. A **41**, 2005 (1990).
[12] D. Asnaghi, M. Carpineti, M. Giglio, and M. Sozzi, Phys. Rev. A **45**, 1018 (1992).
[13] J. P. Wilcoxon, J. E. Martin, and D. W. Shaefer, Phys. Rev. A **39**, 2675 (1989).
[14] B. J. Olivier and C. J. Sorensen, J. Colloid Interface Sci. **134**, 139 (1990).
[15] G. Bolle, C. Cametti, and P. Tartaglia, Phys. Rev. A **35**, 837 (1987).
[16] J. E. Martin, Phys. Rev. A **36**, 3415 (1987).
[17] P. G. J. Van Dongen, and M. H. Ernst, Phys. Rev. Lett. **54**, 1396 (1985).

[18] J. W. Goodwin. The Bristol Polymer Journal, **10**, (1978).
[19] A. Loxley and B. Vincent, Colloid Polym. Sci. **275**, 1108 (1997).
[20] D. D. Perrin, *Dissociation Constants of Organic Bases in Aqueous Solution* (Butterworths, London, 1965).
[21] J. F. Miller, K. Schätzel, and B. Vincent, J. Colloid Interface Sci. **143**, 532 (1991).
[22] A. Fernández-Nieves, A. Fernández-Barbero, B. Vincent, and F. J. de las Nieves, Macromolecules **33**, 2114 (2000).
[23] H. M. Crowther and B. Vincent, Colloid Polym. Sci. **276**, 46 (1998).